Electronic Supplementary Material (ESI) for Physical Chemistry Chemical Physics.

Supporting Information

Effects of strain and thickness on the mechanical, electronic, and optical properties of Cu_2Te

Hangjing Zhou[1,#], Lei Gao[2,#,*], Shihao He[2], Yong Zhang[1], Jianqun Geng[1], Jianchen Lu[1,*], Jinming Cai[1,*]

[1] Faculty of Materials Science and Engineering, Kunming University of Science and Technology, Kunming 650093 China.

[2] Faculty of Science, Kunming University of Science and Technology, Kunming 650500, China.

[#] These authors contributed equally.

[*]Corresponding Authors: lgao@kust.edu.cn, jclu@kust.edu.cn, j.cai@kust.edu.cn.

Table S1 The Calculated Effective Mass (m*), Elastic Modulus (C2D), Deformation Potential Constant El, and Carrier Mobility (μ) of monolayer λ-Cu_2Te and ζ-Cu_2Te

Phase	Direction	Carrier	m*/m0	E1(eV)	C_{2D}(J*m^{-2})	μ($10^3 cm^2V^{-1}S^{-1}$)
ζ-Cu_2Te	x	h	0.18	4.27±0.02	80.04	1.32-1.34
ζ-Cu_2Te	y	h	0.15	5.35±0.01	83.85	1.06-1.07
		e	0.37	3.97±0.02	71.9	2.65-2.67
λ-Cu_2Te		h	0.38	5.35±0.02	82.9	1.64-1.66

Table S2 Theoretical Young's modulus Y (in N/m) and Poisson's ratio v of monolayer λ-Cu_2Te and ζ -Cu_2Te under various strain.

ζ -Cu_2Te	Y(N/m)	v	λ-Cu_2Te	Y(N/m)	v
$\varepsilon_{bia} = -4\%$	96.56–121.17	0.38–0.48	$\varepsilon_{bia} = -4\%$	111.41	0.41
$\varepsilon_{bia} = -2\%$	98.06–110.63	0.38–0.44	$\varepsilon_{bia} = -2\%$	102.04	0.42
$\varepsilon_{bia} = 0\%$	72.08–89.43	0.40–0.51	$\varepsilon_{bia} = 0\%$	90.11	0.43
$\varepsilon_{bia} = 2\%$	63.52–83.26	0.40–0.54	$\varepsilon_{bia} = 2\%$	81.99	0.45
$\varepsilon_{bia} = 4\%$	51.15–68.86	0.42–0.58	$\varepsilon_{bia} = 4\%$	61.22	0.51
$\varepsilon_x = -4\%$	93.36–102.23	0.39–0.43	$\varepsilon_x = -4\%$	71.75–106.75	0.32-0.54
$\varepsilon_x = -2\%$	95.14–101.67	0.38–0.42	$\varepsilon_x = -2\%$	67.21–110.29	0.34−0.51
$\varepsilon_x = 0\%$	82.63–99.22	0.37–0.47	$\varepsilon_x = 0\%$	90.11	0.43
$\varepsilon_x = 2\%$	70.061–97.32	0.36–0.54	$\varepsilon_x = 2\%$	60.76–110.78	0.32−0.60
$\varepsilon_x = 4\%$	62.48–95.401	0.38–0.59	$\varepsilon_x = 4\%$	60.66–108.78	0.31−0.64
$\varepsilon_y = -4\%$	82.96–114.56	0.34–0.51			
$\varepsilon_y = -2\%$	82.72–107.22	0.35–0.49			
$\varepsilon_y = 0\%$	81.758–98.91	0.37–0.47			
$\varepsilon_y = 2\%$	78.528–91.16	0.39–0.47			

$\varepsilon_y = 4\%$	68.292–84.91	0.41–0.52

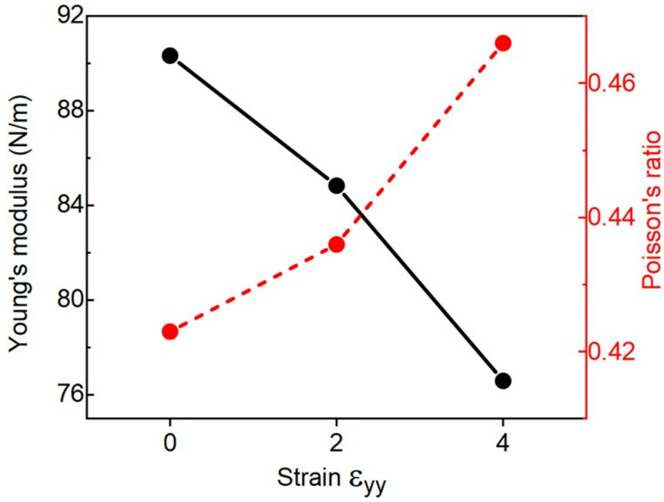

Fig. S1 Orientation-dependent Young's modulus and Poisson's ratio v of monolayer ζ-Cu_2Te calculated under various values of strain (ε = -2%, 0%, 2%).

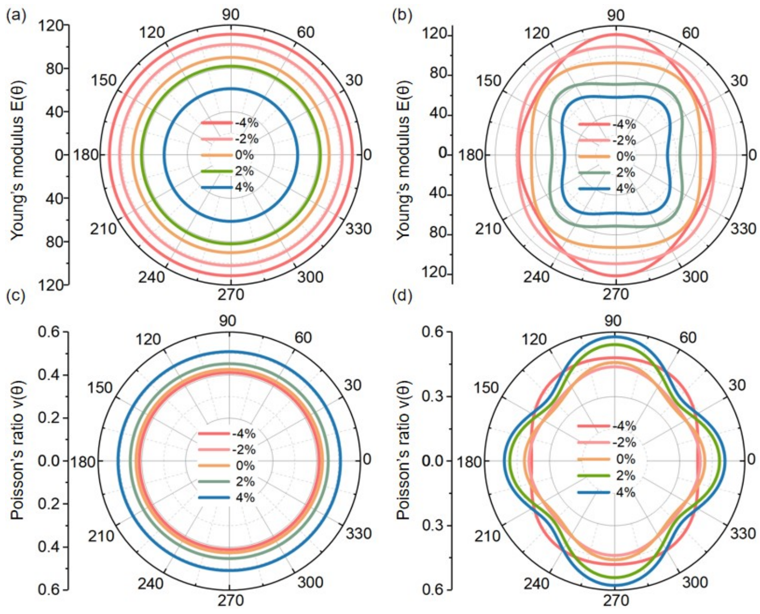

Fig. S2 Orientation-dependent in-plane Young's modulus and Poisson's ratio for 2D monolayer λ-Cu_2Te (a, d) and ζ-Cu_2Te (b, c) under various biaxial compressive and tensile strains.

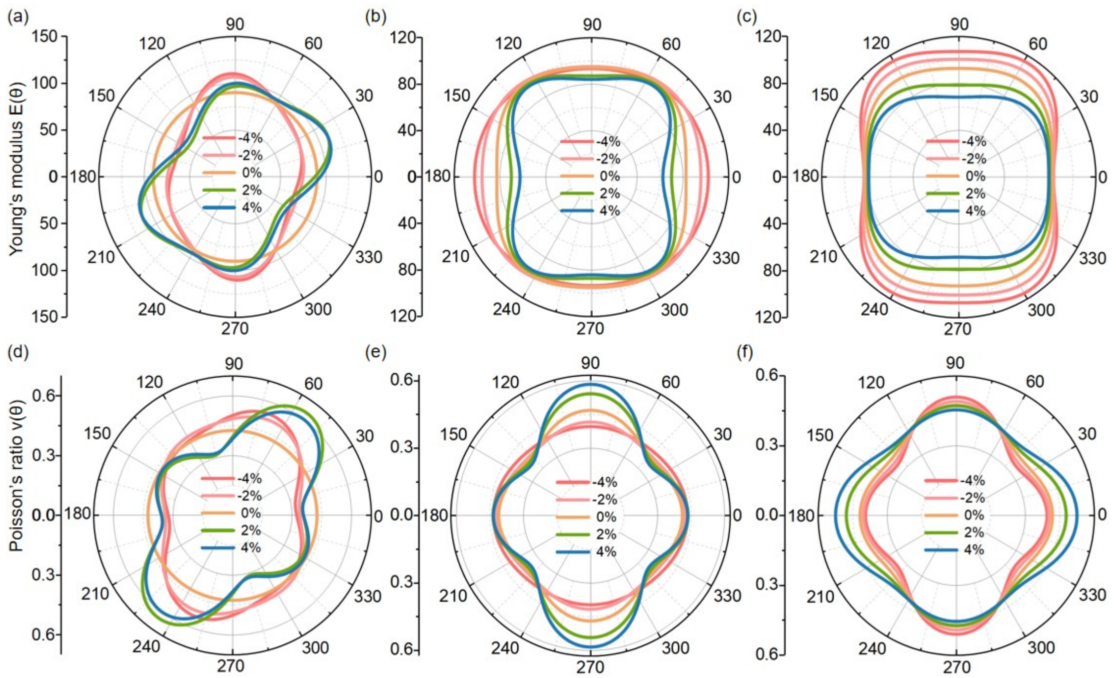

Fig. S3 Orientation-dependent in-plane Young's modulus and Poisson's ratio for 2D monolayer λ-Cu_2Te under x-directional strains (a, d) and ζ-Cu_2Te under various compressive and tensile strains along the x- (b, e) and y-directions (c, f).

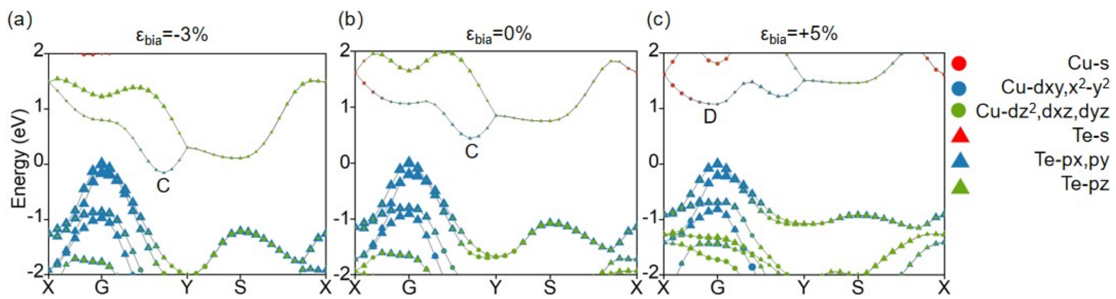

Fig. S4 Projection energy band structures of ζ-Cu_2Te corresponding to various biaxial strain values (a) $\varepsilon = -3\%$, (b) 0% and (c) 5% through HSE06 calculations.

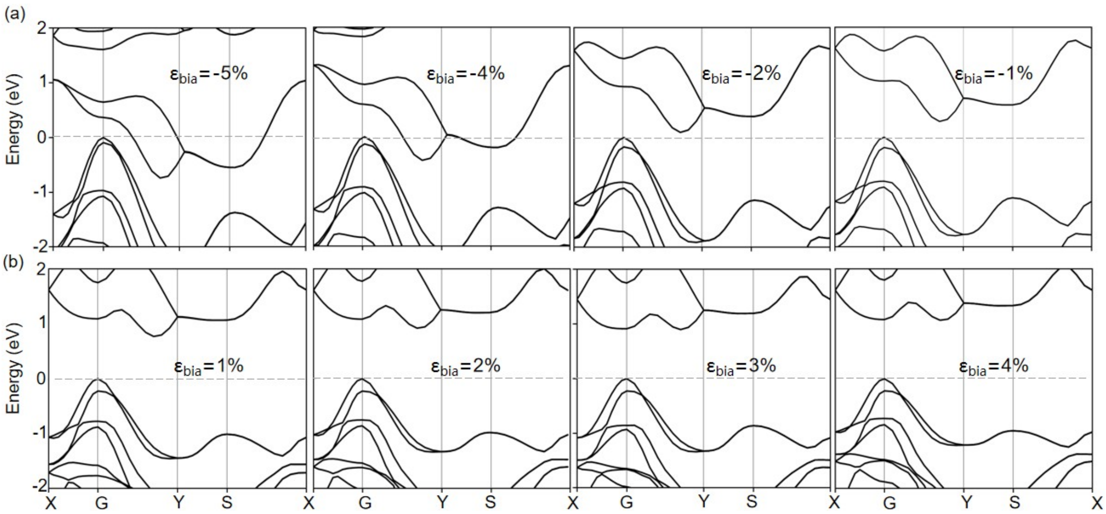

Fig. S5 Calculated (a) biaxial compressive strain– and (b) biaxial tensile strain–dependent electronic band structures of monolayer ζ-Cu_2Te obtained through HSE06 calculations.

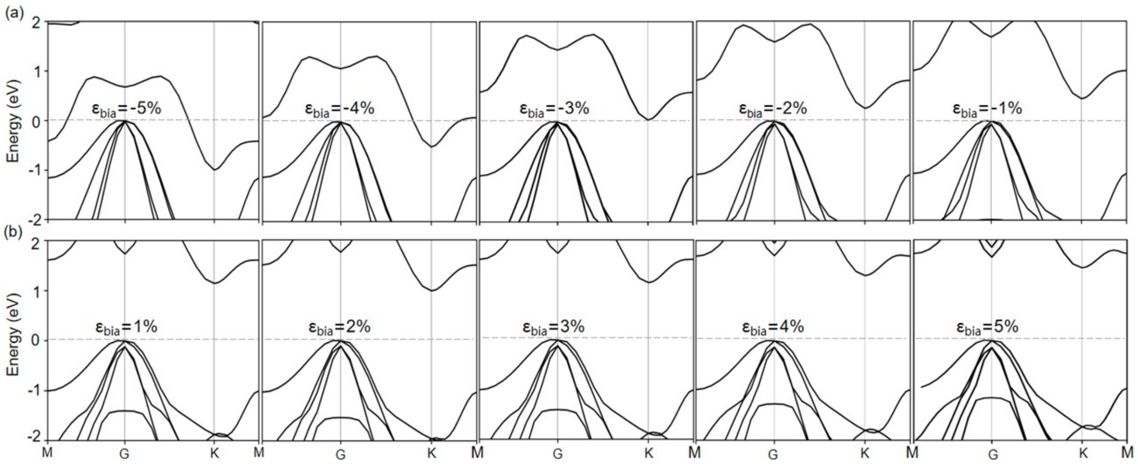

Fig. S6 Calculated (a) biaxial compressive strain– and (b) biaxial tensile strain–dependent electronic band structures of monolayer λ-Cu_2Te obtained through HSE06 calculations.

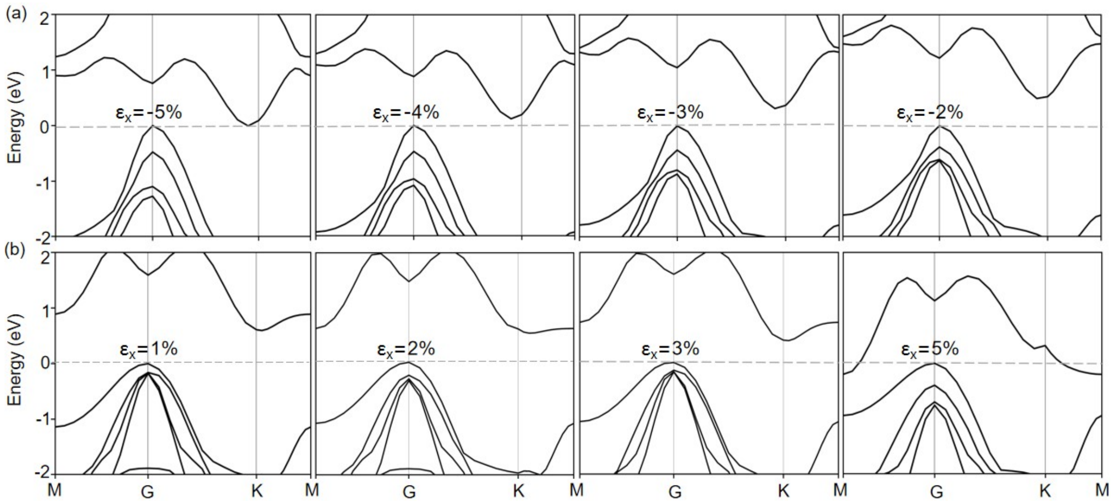

Fig. S7 Calculated (a) uniaxial compressive strain– and (b) uniaxial tensile strain–dependent electronic band structures of monolayer λ-Cu_2Te obtained through HSE06 calculations.

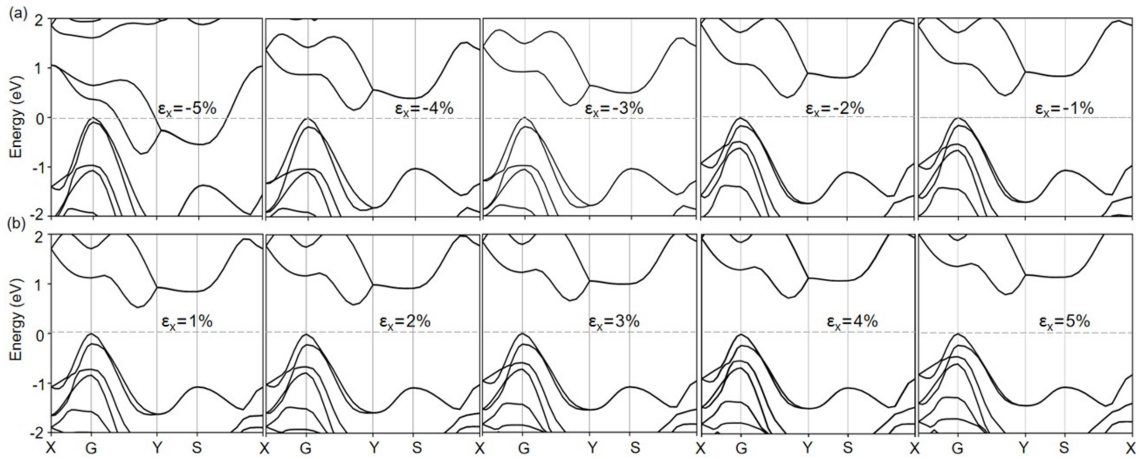

Fig. S8 Calculated (a) uniaxial compressive strain– and (b) uniaxial tensile strain–dependent electronic band structures of monolayer ζ-Cu_2Te obtained through HSE06 calculations.

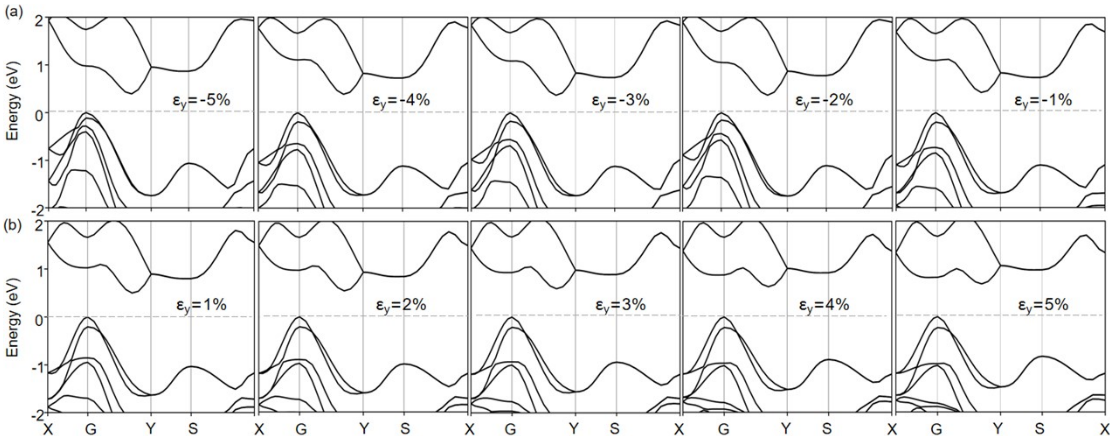

Fig. S9 Calculated (a) uniaxial compressive strain– and (b) uniaxial tensile strain–dependent electronic band structures of monolayer ζ-Cu_2Te obtained through HSE06 calculations.

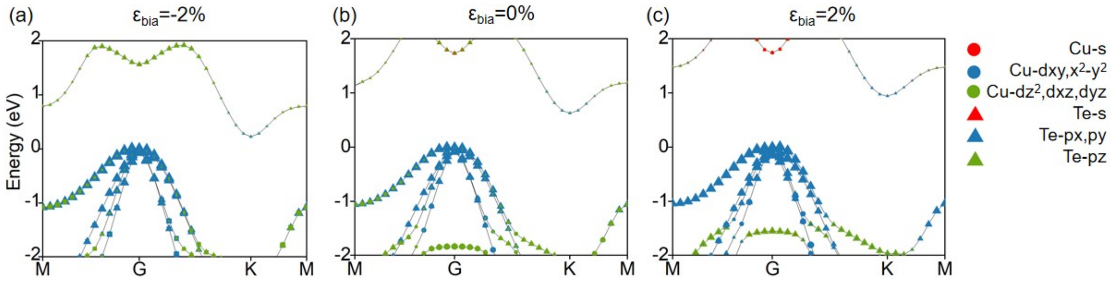

Fig. S10 Projection energy band structures of λ-Cu_2Te corresponding to various biaxial strain values (a) ε = –2%, (b) 0% (c) 2%, through HSE06 calculations.

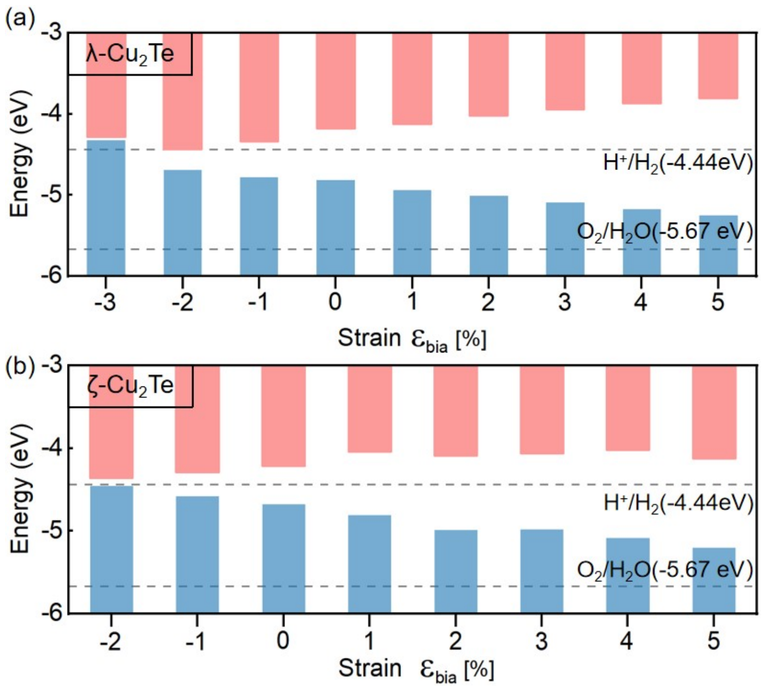

Fig. S11 Band-edge alignment of monolayer (a) λ-Cu_2Te and (b) ζ-Cu_2Te under various biaxial strain through HSE06 calculations with respect to the vacuum level. The gray dashed lines denote the water potential of water.

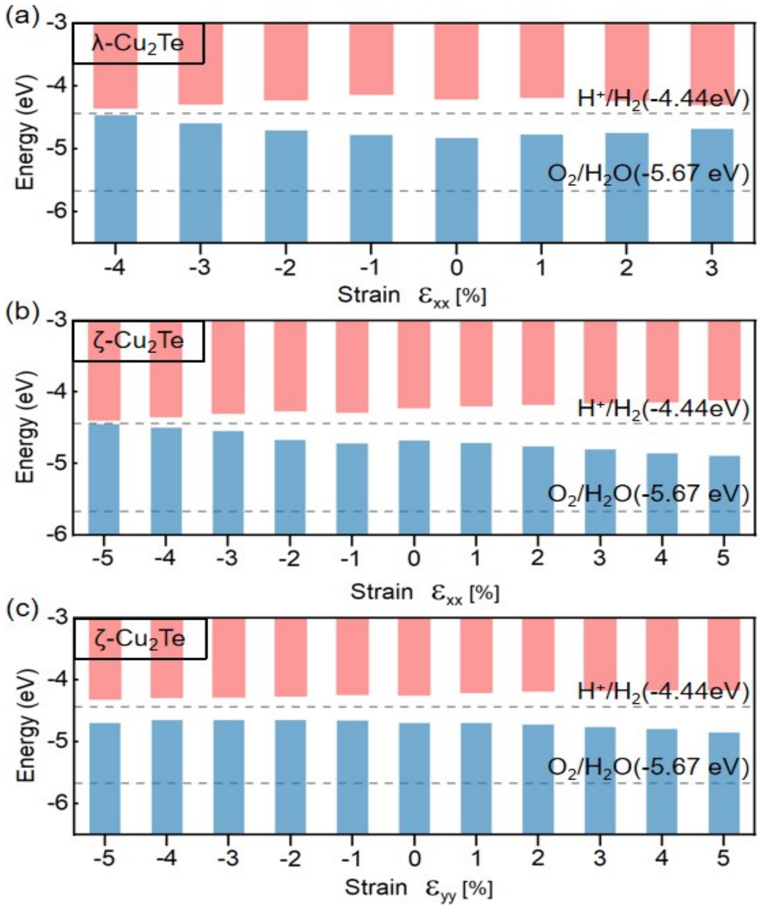

Fig. S12 Band-edge alignment of monolayer (a) λ-Cu_2Te and (b, c) ζ-Cu_2Te under various uniaxial strain through HSE06 calculations with respect to the vacuum level. The gray dashed lines denote the redox potential of water.

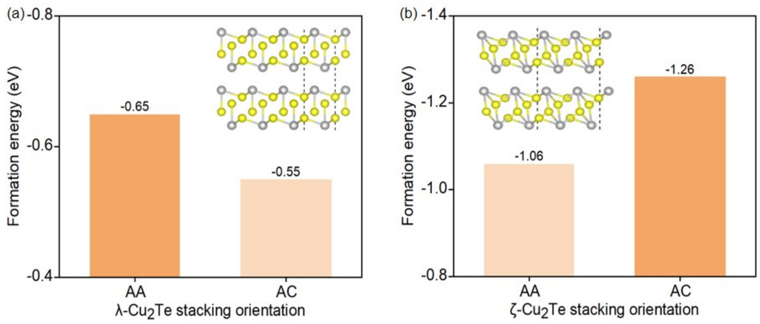

Fig. S13 Calculated formation energies of 2L (a) λ-Cu_2Te and (b) ζ-Cu_2Te. Side views of the structures of λ-Cu_2Te and ζ-Cu_2Te are also shown.

Table S3 Theoretical Young's modulus Y (in N/m) and Poisson's ratio v of few-layered λ-Cu_2Te and ζ-Cu_2Te.

	Y (N/m)	v
ζ-Cu_2Te		
2-Layers	171.20–196.18	0.40–0.47
3-Layers	246.54–288.27	0.39–0.47
λ-Cu_2Te		
2-Layers	184.12	0.47
3-Layers	286.54	0.43

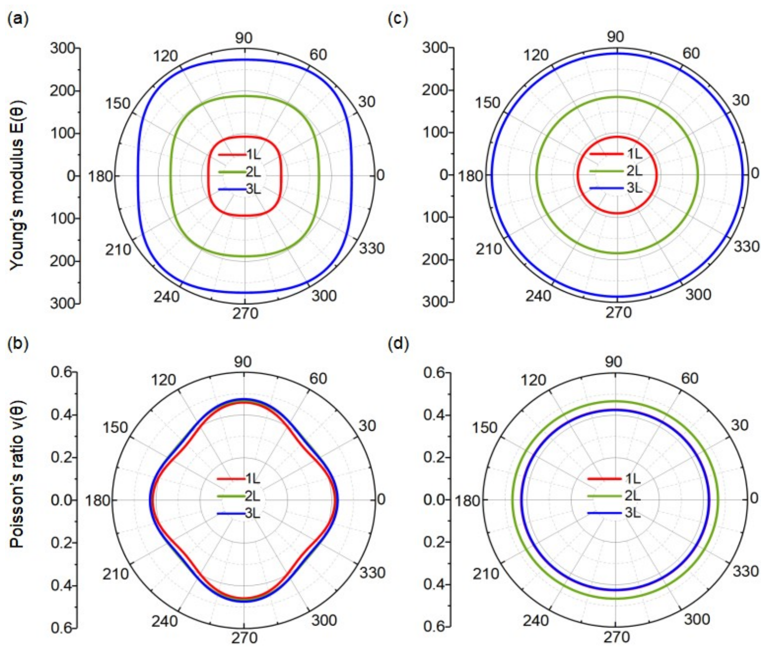

Fig. S14 Young's modulus and Poisson's ratio of (a, b) ζ-Cu_2Te and (c, d) λ-Cu_2Te. Both are functions of the in-plane angle θ.

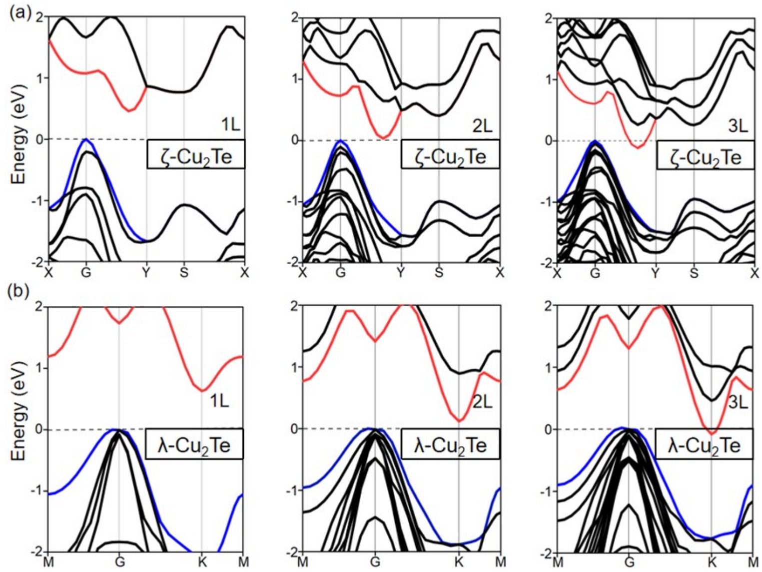

Fig. S15 Band structure of (a) λ-Cu_2Te and (b) ζ-Cu_2Te with the number of layers ranging from 1 to 3, through HSE06 calculations.

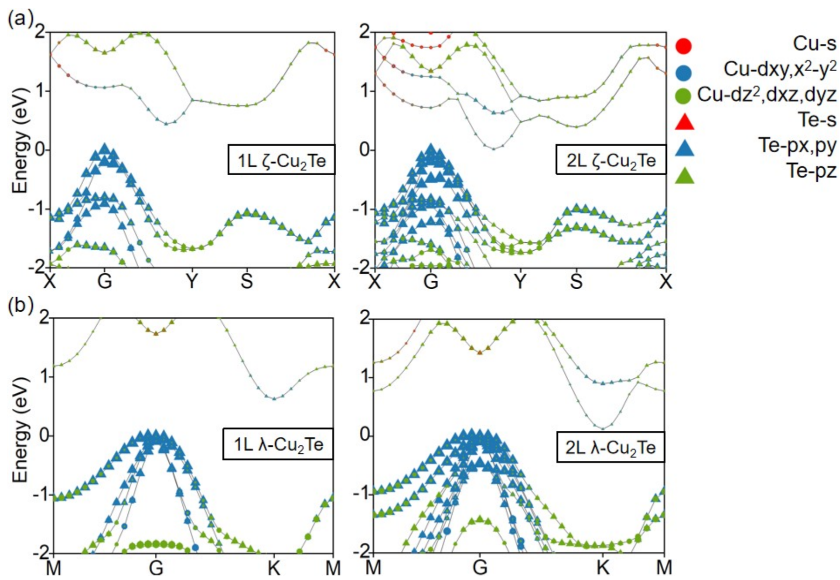

Fig. S16 Thickness-dependent projection energy band structures in few-layer (a) ζ-Cu_2Te and (b) λ-Cu_2Te obtained through HSE06 calculations.